energies

MDPI

Article

Characterization of Bio-Adsorbents Produced by Hydrothermal Carbonization of Corn Stover: Application on the Adsorption of Acetic Acid from Aqueous Solutions

Maria Elizabeth Gemaque Costa [1], Fernanda Paula da Costa Assunção [2], Tiago Teribele [1], Lia Martins Pereira [1], Douglas Alberto Rocha de Castro [1], Marcelo Costa Santo [1], Carlos Emerson Ferreira da Costa [3], Maja Shultze [4], Thomas Hofmann [4] and Nélio Teixeira Machado [1,4,5,*]

1 Graduate Program of Natural Resources Engineering of Amazon, Rua Augusto Corrêa N° 1, Campus Profissional-UFPA, Belém 66075-110, Brazil; gemaquebeth@yahoo.br (M.E.G.C.); teribele@globo.com (T.T.); liapereira@ufpa.br (L.M.P.); douglascastro87@hotmail.com (D.A.R.d.C.); marcelo.santos@ufra.edu.br (M.C.S.)
2 Graduate Program of Civil Engineering, Rua Augusto Corrêa N° 1, Campus Profissional-UFPA, Belém 66075-110, Brazil; fernanda.assuncao.itec@gmail.com
3 Graduate Program of Chemistry, Rua Augusto Corrêa N° 1, Campus Profissional-UFPA, Belém 66075-110, Brazil; emmerson@ufpa.br
4 Department of Postharvest Technology, Leibnitz-Institüt für Agrartechnik Potsdam-Bornin e.V, Max-Eyth-Alee 100, 14469 Potsdam, Germany; mschultze@atb-potsdam.de (M.S.); THoffmann@atb-potsdam.de (T.H.)
5 Faculty of Sanitary and Environmental Engineering, Rua Corrêa N° 1, Campus Profissional-UFPA, Belém 66075-900, Brazil
* Correspondence: machado@ufpa.br; Tel.: +55-91-984-620-325

Abstract: In this work, the influence of temperature on textural, morphological, and crystalline characterization of bio-adsorbents produced by hydrothermal carbonization (HTC) of corn stover was systematically investigated. HTC was conducted at 175, 200, 225, and 250 °C, 240 min, heating rate of 2.0 °C/min, and biomass-to-H_2O proportion of 1:10, using a reactor of 18.927 L. The textural, morphological, crystalline, and elemental characterization of hydro-chars was analyzed by TG/DTG/DTA, SEM, EDX, XRD, BET, and elemental analysis. With increasing process temperature, the carbon content increased and that of oxygen and hydrogen diminished, as indicated by elemental analysis (C, N, H, and S). TG/DTG analysis showed that higher temperatures favor the thermal stability of hydro-chars. The hydro-char obtained at 250 °C presented the highest thermal stability. SEM images of hydro-chars obtained at 175 and 200 °C indicated a rigid and well-organized fiber structure, demonstrating that temperature had almost no effect on the biomass structure. On the other hand, SEM images of hydro-chars obtained at 225 and 250 °C indicated that hydro-char structure consists of agglomerated micro-spheres and heterogeneous structures with nonuniform geometry (fragmentation), indicating that cellulose and hemi-cellulose were decomposed. EDX analysis showed that carbon content of hydro-chars increases and that of oxygen diminish, as process temperature increases. The diffractograms (XRD) identified the occurrence of peaks of higher intensity of graphite (C) as the temperature increased, as well as a decrease of peaks intensity for crystalline cellulose, demonstrating that higher temperatures favor the formation of crystalline-phase graphite (C). The BET analysis showed 4.35 m^2/g surface area, pore volume of 0.0186 cm^3/g, and average pore width of 17.08 µm. The solid phase product (bio-adsorbent) obtained by hydrothermal processing of corn stover at 250 °C, 240 min, and biomass/H_2O proportion of 1:10, was activated chemically with 2.0 M NaOH and 2.0 M HCl solutions to investigate the adsorption of CH_3COOH. The influence of initial acetic acid concentrations (1.0, 2.0, 3.0, and 4.0 mg/mL) was investigated. The kinetics of adsorption were investigated at different times (30, 60, 120, 240, 480, and 960 s). The adsorption isotherms showed that chemically activated hydro-chars were able to recover acetic acid from aqueous solutions. In addition, activation of hydro-char with NaOH was more effective than that with HCl.

Keywords: corn stover; hydrothermal process; hydrochar; adsorption; acetic acid; thermo-gravimetric analysis; scanning electron microscopy; X-ray diffraction; BET analysis

Citation: Costa, M.E.G.; da Costa Assunção, F.P.; Teribele, T.; Pereira, L.M.; de Castro, D.A.R.; Santo, M.C.; da Costa, C.E.F.; Shultze, M.; Hofmann, T.; Machado, N.T. Characterization of Bio-Adsorbents Produced by Hydrothermal Carbonization of Corn Stover: Application on the Adsorption of Acetic Acid from Aqueous Solutions. *Energies* **2021**, *14*, 8154. https://doi.org/10.3390/en14238154

Academic Editor: Andrea Di Carlo

Received: 15 October 2021
Accepted: 3 November 2021
Published: 5 December 2021

1. Introduction

Hydro-char is porous carbonaceous material with reactive, functionalized/aromatic surfaces [1]. These morphological and textural properties make hydrochar a potential adsorbent to remove/recover chemical contaminants from process water [1–5], until the process aqueous phase produced by hydrothermal carbonization of biomass [6]. Hydrochars differ from biochars due to its lower aromaticity, consisting of mostly alkyl moieties [7]. In recent years, the literature reports the application of hydro-chars as bio-adsorbents to selectively remove organic and inorganic compounds, as well as heavy metal, that is, the adsorption/sorption of aqueous contaminants onto hydro-chars [1–6,8–51].

Hydro-chars have been applied as adsorbents due to their capacity to remove and or selectively absorb polar and non-polar organic compounds, including acetic acid [6], bisphenol A, 17α-ethinyl estradiol and phenanthrene [22], 2-naphthol [11], pyrene [22]; phenolic compounds (phenol, guaiacol, vanillyl alcohol, and resorcinol) [31]; dyes, such as methylene blue [8,9,23,24,26,27,29,36,38–47], methyl orange [36,49], methylene green [48], and Congo red [11]; herbicides, such as fluridone, norflurazon [18], and isoproturon [19]; pharmaceuticals, such as triclosan, estrone, carbamazepine, acetaminophen [12], sulfamethoxazole, diclofenac, bezafibrate, carbamazepine, atrazine [16,51], tetracycline [20], diclofenac sodium, salicylic acid, and flurbiprofen [21]; alkaline (K^+, Na^+) and alkaline earth metals (Mg^{2+}, Ca^{2+}) [31]; heavy metals, such as lead [2–4,10,15,23–25,28,30,32,42], cadmium (II) [2,4,5,10,13,24,32,38], uranium(VI) [1,35], antimony [13], copper(II) [4,5,10,14,17,24,39,50], nickel [4], zinc [10], and chromium(II) [33]; and fertilizers such as phosphate [23,34], orthophosphate [50], and ammonium [34].

The chemical activation of hydro-chars was carried out by either modifying the reaction media composition (H_20 + *modifier*) or the solid phase reaction products (hydro-char + modifier) and has been intensively investigated in recent years [4,8–10,21,26–30,32,33,35,36,38–43,45–51]. The physical activation of hydrochars has also been investigated [24]. Changes in the mesoporous and surface properties of hydro-chars by modifying the reaction medium composition include the addition of H_3PO_4 (phosphoric acid) [30], CH_2 = CH-COOH (acrylic acid) [29,32], terminal amino hyper-branched polymer solutions [33], $C_2H_2(CO)_2O$ (maleic anhydride) followed by deprotonation of carboxyl groups with $NaHCO_3$ solution [35], $ZnCl_2$ (zinc chloride) [41], NaOH [48], HCl, NaOH, and NaCl [51]. In addition, hydro-char mesoporous and surface properties have been chemically activated with H_2O_2 [4,25], NaOH [6,8,9,26,27,29], KOH [10,28,47,50], H_3PO_4 [21], polyaminocarboxylated modified hydro-char [39], O_3/NaCl [42], HNO_3 [43], and until etherification, amination and protonation reaction [49].

The water process streams by hydrothermal carbonization of lignocellulosic materials is a complex mixture containing aromatic-ring compounds (furfural, HMF, phenols, cresols, catechol, and guaiacol) [52–54], carboxylic acids (formic acid, acetic acid, propionic acid, and lactic acid) [52–54], alcohols (methanol and ethanol) [52,53], and sugars [54], with high concentrations of volatiles carboxylic acids [52–54], as well as hazardous substances such as HMF (hydromethylfurfural), thus making its reuse, even as washing water not possible, so that application of separation processes is necessary to recover organic and inorganic compounds. In addition, Machado et al. [52] stated that complex chemical composition of water process streams by HTC poses a hard separation task, because of the huge differences in chemical structure, as well as thermal and physical properties such as boiling point. In fact, many of those compounds present boiling points higher than H_2O, so that application of separation processes (except adsorption [6,31]), such as distillation and evaporation are not effective [52].

Despite some studies on the adsorption/sorption of organic compounds within hydrochar produced by hydrothermal carbonization of biomass, activated chemically with NaOH [6,8,9,26,27,29], only a few have investigated the uptake of organic compounds from aqueous process streams from hydrothermal carbonization/liquefaction [6,31], as summarized synthetically below. In addition, until now, no study has investigated the adsorption of acetic acid in hydro-char activated chemically with HCl.

Machado et al. [6], studied the adsorption of acetic acid form H_2O solutions on hydro-chars produced by hydrothermal carbonization of corn stover at 200, 225, and 250 °C, 240 min, heating rate of 2 °C/min, biomass/H_2O proportion of 1:10, using a reactor of 18.927 L, in batch mode. The hydro-chars were characterized by SEM, EDX, and XRD [6]. The hydro-char obtained at 250 °C, was activated chemically with a 2.0 M NaOH solution [6]. The influence of initial CH_3COOH concentrations on the adsorption kinetic was investigated [6]. The adsorption kinetics was investigated at 30, 60, 120, 240, 480, and 960 s [6]. The adsorption isotherms showed that chemically activated hydro-chars were able to recover acetic acid from aqueous solutions [6].

Sanette et al. [31], investigated the adsorption of AAEMs (alkaline and alkaline earth metals) (Ca^{2+}, K^+, Na^+, and Mg^{2+}), as well as phenolic compounds (guaiacol, phenol, vanillyl alcohol, and resorcinol) present in process water streams obtained by hydrothermal carbonization of a model (synthetic) mixture that mimics the organic fraction of municipal solid waste at 300 °C, 15 min, feedstock/H_2O proportion of 1:1, using a stainless steel reactor of 945 mL, on chemically activated hydro-char with KOH solutions of concentrations between 0.5 and 2.5 mol/L. For AAEM the order of adsorption was $Ca^{2+} > K^+ > Na^+ > Mg^{2+}$ [31]. The synthetic hydro-char was able to uptake 100% of guaiacol, phenol, and resorcinol and 61% of vanillyl alcohol present in process water streams [31]. The multilayer adsorption of phenolic compounds was correlated using the Dubinin-Radushkevich isotherm, showing equilibrium adsorbent-phase loadings of 68.7 mg/g and 50.3 mg/g for vanillyl alcohol and resorcinol, respectively [31]. On the other hand, Henry's law best correlated the adsorption of AAEMs [31].

In this work, the influence of process temperature on the textural, morphological, and crystalline characterization of hydro-chars produced by hydrothermal carbonization of corn stover at 175, 200, 225, and 250 °C, 240 min, heating rate of 2.0 °C/min, and biomass/H_2O proportion of 1:10, using a reactor of 18.927 L, was investigated systematically. In addition, this work also investigated the influence of alkali (NaOH) and acid (HCl) pre-treatment over the hydro-char produced at 250 °C, on the adsorption/sorption of acetic acid (CH_3COOH) on hydro-char by analyzing the effect of initial concentration of acetic acid (CH_3COOH), as well as acetic acid solution-to-adsorbent ratio on the adsorption kinetics, adsorption equilibrium, and sorption equilibrium capacity in laboratory scale, batch mode.

2. Materials and Methods

2.1. Methodology

Figure 1 outlines the methodology as a rational scheme of ideas, methods, and procedures to produce the bio-adsorbent. The chemically activated adsorbent was applied to uptake acetic acid from aqueous solutions. Initially, the corn stover was collected. Afterwards, it was submitted to pretreatments of drying, grinding and sieving. The hydrothermal carbonization was carried out in batch mode, closed system, and pilot scale, as described elsewhere [52]. The hydro-chars were characterized by TG/DTG/DTA, SEM/EDX, BET, and XRD. The hydro-char were obtained by processing of corn stover with hot compressed H_2O at 250 °C, chemically activated with NaOH and HCl. The adsorption of acetic acid (CH_3COOH) on hydro-char was investigated by analyzing the adsorption kinetics, adsorption equilibrium, and sorption equilibrium capacity in laboratory scale, batch mode.

2.2. Materials, Pre-Treatment, and Physicochemical Characterization of Corn Stover

The corn stover was supplied by ATB-Bornin [52]. The residues were pretreated by drying, grinding, and sieving, as described elsewhere [52]. Afterwards, the residues were physicochemically characterized for dry matter, organic matter, ash, and elemental analysis, while oxygen was computed by difference, as described elsewhere [52].

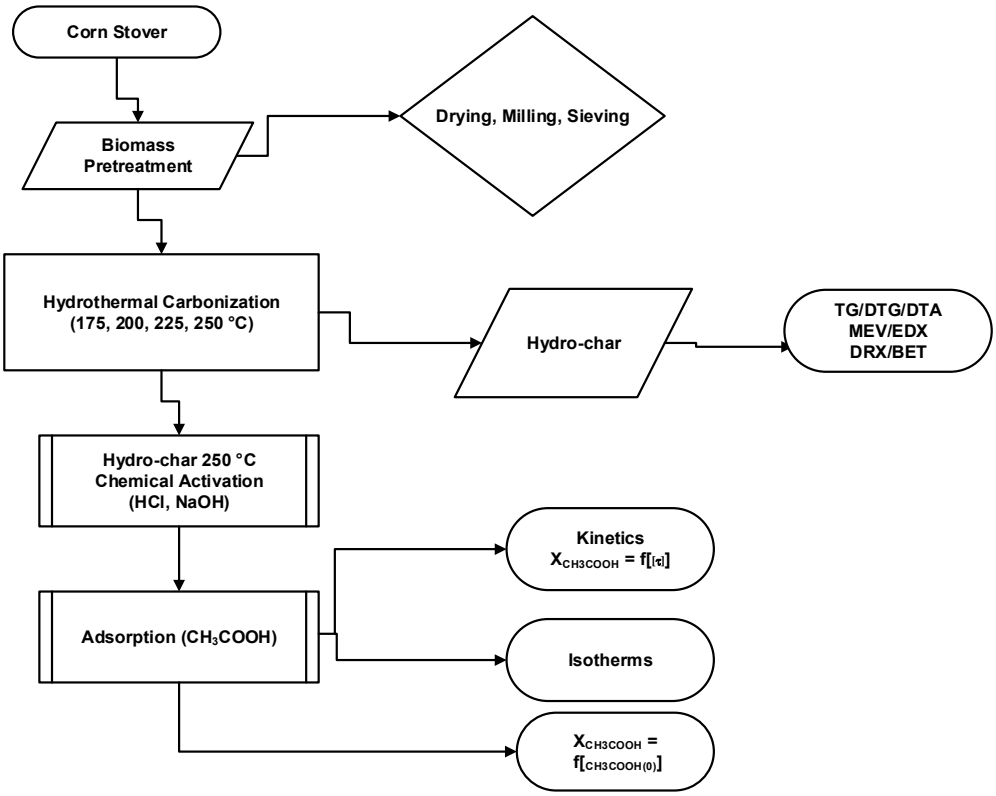

Figure 1. Process diagram of adsorption of acetic acid on hydro-char chemically activated with NaOH and HCl, obtained by HTC of corn stover at 250 °C, 240 min, and biomass/H_2O proportion of 1:10, batch mode, closed system, in pilot scale.

2.3. Experimental Apparatus and Procedures

Hydrothermal Carbonization

The experiments were performed at 175, 200, 225, and 250 °C, 240 min, and biomass/H_2O proportion of 1:10, using a reactor of 18.927 L, and the apparatus and procedures described elsewhere [52].

2.4. Adsorption of CH_3COOH

The adsorption kinetic of acetic acid into hydro-char produced by hydrothermal carbonization of corn stover at 250 °C, 240 min, biomass/H_2O proportion of 1:10, in pilot scale, chemically activated with NaOH and HCl, was investigated systematically. The uptake of CH_3COOH can be investigated by determining the acetic acid solution initial concentration $C^L_{CH3COOH}(0)$ and the concentrations of CH_3COOH in aqueous solutions at time (τ) $C^L_{CH3COOH}(\tau)$, until the time reaches its minimum value at (∞), that is, the acetic acid concentration in aqueous phase at equilibrium with hydro-char $C^L_{CH3COOH}(\infty)$ [6].

In cases, where only one organic acid specie is solvated in water (model solution), it is possible to determine the concentration of an organic acid in water by computing the acid value, as the proportion acidity/concentration of acetic acid ($C^L_{CH3COOH}$) is constant, given by Equation (1).

Applying a steady-state mole balanced, closed, and conservative system for the adsorption analysis (acetic acid aqueous solution (liquid phase) + hydro-char (solid phase)), the quantity of moles of acetic acid in water at the beginning n^L_0 is equal to quantity of moles of acetic acid in water at time (τ) n^L_τ and quantity of moles of acetic acid uptake into hydro-char at time (τ) n^S_τ defined by Equation (2). Dividing Equation (1) by solution volume V yields Equation (3), where $C^L_{CH3COOH}(0)$ is the initial acetic acid solution concentration, $C^L_{CH3COOH}(\tau)$ the acetic acid solution concentration at time (τ), and $C^S_{CH3COOH}(\tau)$ the acetic acid concentration in hydro-char at time (τ).

The acetic acid concentration in hydro-char at time (τ) is given by Equation (4). By substituting the relation given by Equation (1) in Equation (4), it is possible to compute, indirectly, the acetic acid concentration in hydro-char at time (τ), by the difference between the initial solution acid value $I^{L}_{CHeCOOH}(0)$ and the solution acid value at time (τ), $I^{L}_{CH3COOH}(\tau)$.

When acetic acid concentration in water reaches equilibrium, that is, $C^{L}_{CH3COOH}(\infty) = C^{*}_{CH3COOH}$, $I^{L}_{CH3COOH}(\infty) = I^{*}_{CH3COOH}$, the acetic acid concentration into hydro-char reaches its maximum at equilibrium $C^{S}_{CH3COOH}(\infty) = C^{*}_{CH3COOH}$, and the difference $I^{L}_{CH3COOH}(0) - I^{L}_{CH3COOH}(\infty)$, Equation (5), reaches its maximum.

$$I^{L}_{CH3COOH} \propto C^{L}_{CH3COOH},\ I^{L}_{CH3COOH} = K * C^{L}_{CH3COOH} \quad (1)$$

$$n^{L}_{0} = n^{L}_{\tau} + n^{S}_{\tau} \quad (2)$$

$$C^{L}_{CH3COOH}(0) = C^{L}_{CH3COOH}(\tau) + C^{S}_{CH3COOH}(\tau) \quad (3)$$

$$C^{S}_{CH3COOH}(\tau) = C^{L}_{CH3COOH}(0) - C^{L}_{CH3COOH}(\tau),\ I(\tau) = I^{L}_{CH3COOH}(0) - I^{L}_{CH3COOH}(\tau) \quad (4)$$

$$C^{S}_{CH3COOH}(\infty) = C^{*}_{CH3COOH},\ I^{*} = I^{L}_{CH3COOH}(0) - I^{L}_{CH3COOH}(\infty) \quad (5)$$

A first order kinetic was applied to describe the adsorption process, expressed as a dimensionless acidity, given by Equation (6).

$$I(\tau) = I^{L}_{CHeCOOH}(0) * [1 - \exp(-K * \tau)] \quad (6)$$

where K, is the adsorption kinetic constant.

2.4.1. Adsorption Isotherm of CH_3COOH

The Langmuir isotherm, given by Equation (7), was applied to analyze the adsorption equilibrium data of acetic acid in aqueous solutions within a porous solid matrix (adsorbent), where $\chi^{*}_{CH3COOH}$ is the equilibrium adsorbent-phase concentration of CH_3COOH, $C^{*}_{CH3COOH}$, is the equilibrium aqueous-phase concentration of acetic acid, and K_0, χ_{Max}, the adsorption equilibrium constant and the saturation adsorption loading, respectively.

$$\chi^{*}_{CH3COOH} = \frac{K_0 * \chi_{Max} * C^{*}_{CH3COOH}}{(1 + K_0 * C^{*}_{CH3COOH})} \quad (7)$$

2.4.2. Adsorption Apparatus and Procedures

The adsorption apparatus and procedures of CH_3COOH on hydro-char activated with NaOH (2.0 M) and HCl (2.0 M), was described in detail by Machado et al. [6].

2.5. Morphological, Crystalline, and Textural Characterization of Hydro-Chars

The morphological, crystalline, and textural characterization of hydro-chars obtained by hydrothermal processing of corn stover at 175, 200, 225, and 250 °C, 240 min, and biomass/H_2O proportion of 1:10, using a reactor of 18.927 L, was performed by SEM, EDX, and XRD (the equipment and procedures were described elsewhere [55,56]) as well as by thermo-gravimetric analysis (TG/DTG/DTA) and BET [56].

Thermo-Gravimetric Analysis (TG/DTG/DTA)

The weight loss of hydro-chars obtained by hydrothermal processing of corn stover at 175, 200, 225, and 250 °C, 240 min, and biomass/H_2O proportion of 1:10, using a reactor of 18.927 L, was analyzed by TG/DTG/DTA, and the equipment and procedures were described elsewhere [57].

3. Results

3.1. Morphological, Crystalline, and Textural Characterization of Hydro-Chars

3.1.1. Thermo-Gravimetric Analysis (TG/DTG/DTA)

Sittisun et al. [58], studied the thermal degradation of corn stover between 25 and 900 °C, heating rates of 10, 20, and 50 °C/min. The authors reported for heating rates of 10 °C/min, a mass loss of approximately 92 (wt.%), between 25 and 510 °C.

In the temperature region 510–900 °C, the mass loss was constant, and the remaining solid phase was composed of ash. The DTG curve shows three different thermal degradation steps. In the first one, between 25 and 167 °C, a mass loss of 8.5 (wt.%) was reported, representing the recovery of moisture within the solid phase. Afterwards, in the temperature region 167–368 °C, a mass loss of 56.59 (wt.%) occurred, mainly due to release of volatile compounds by the degradation reactions of cellulose and hemi-cellulose, described chemically by degradation of chemical functions containing oxygen, including hydroxyl, carbonyl, and carboxyl groups [58,59]. In the last step, between 368 and 514 °C, a mass loss of 26.50 (wt.%) occurred, associated with the thermal degradation and/or combustion of lignin, as well as residual char compounds, produced at the second step.

Figures 2–4 describe the TG, DTG, and DTA analysis of corn stover after hydrothermal processing at 175, 200, 225, and 250 °C, 240 min, and biomass/H_2O proportion of 1:10, respectively, using a reactor of 18.927 L, between 25 and 800 °C, 10 °C/min, under N_2 atmosphere.

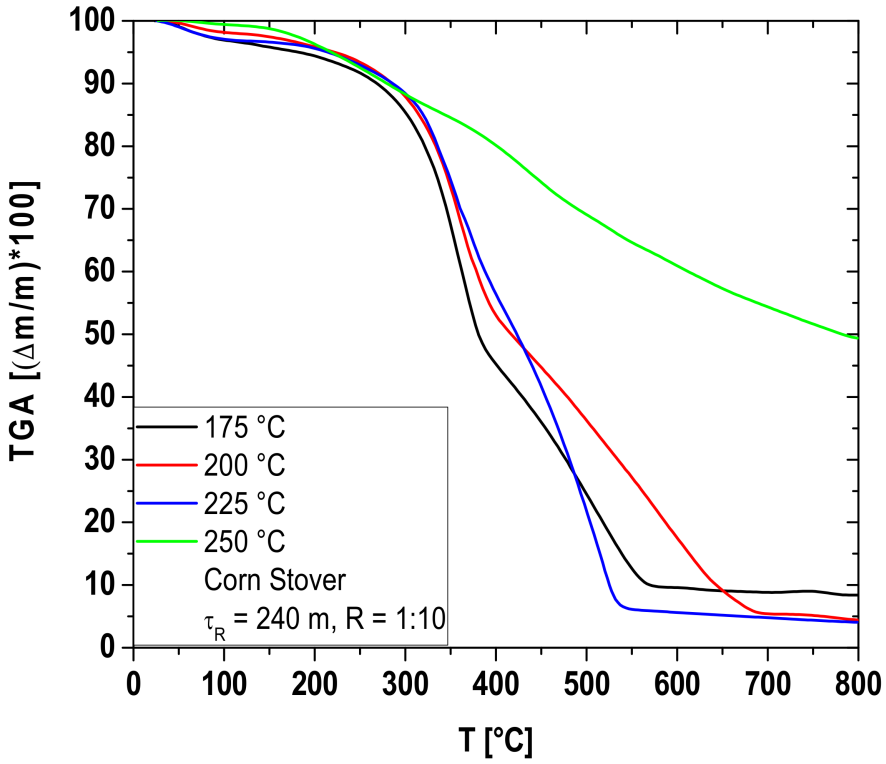

Figure 2. TG of hydro-chars obtained by hydrothermal carbonization of corn stover at 175, 200, 225, and 250 °C, 240 min, and biomass/H_2O proportion of 1:10, using a reactor of 18.927 L.

One observes, for the thermal degradation of corn stover after hydrothermal processing at 175 °C, the occurrence of 03 reaction steps. In the first one, between 25 and 150 °C, a mass loss of approximately 3.0–4.0 (wt.%) occurred, due to the release of moisture. It is also probable that degradation of volatile compounds selectively adsorbed into the pores of solid phase products has taken place, including alcohols (methanol, ethanol), carboxylic acids (acetic acid, propanoic acid) [6], and aldehydes (HMF). In the second degradation step, between 150 and 530 °C, a mass loss of approximately 79–80 (wt.%) occurred.

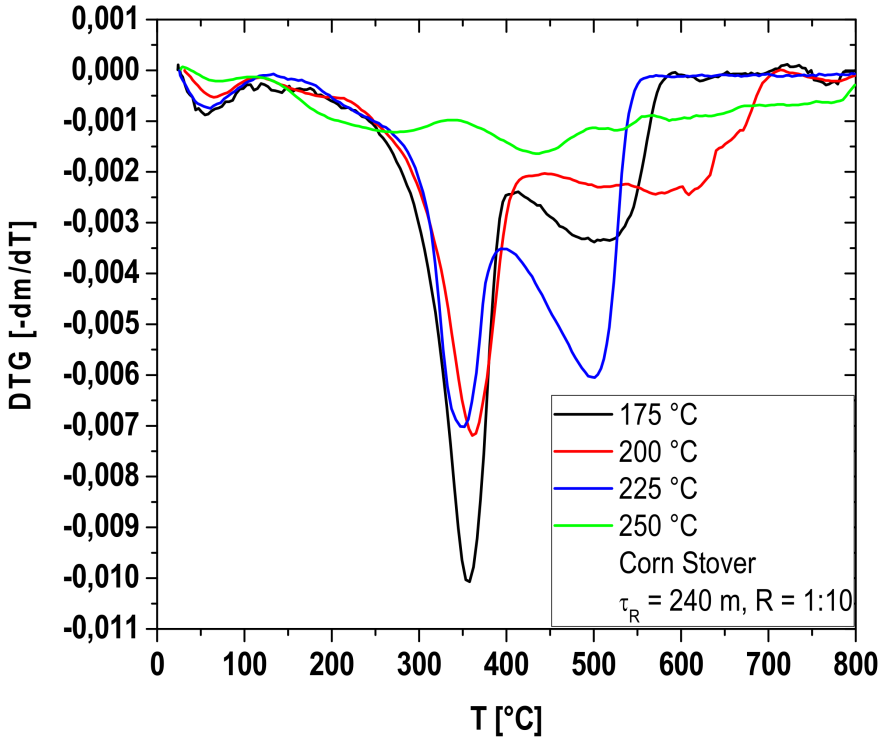

Figure 3. DTG of hydro-chars obtained by hydrothermal carbonization of corn stover at 175, 200, 225, and 250 °C, 240 min, and biomass/H_2O proportion of 1:10, using a reactor of 18.927 L.

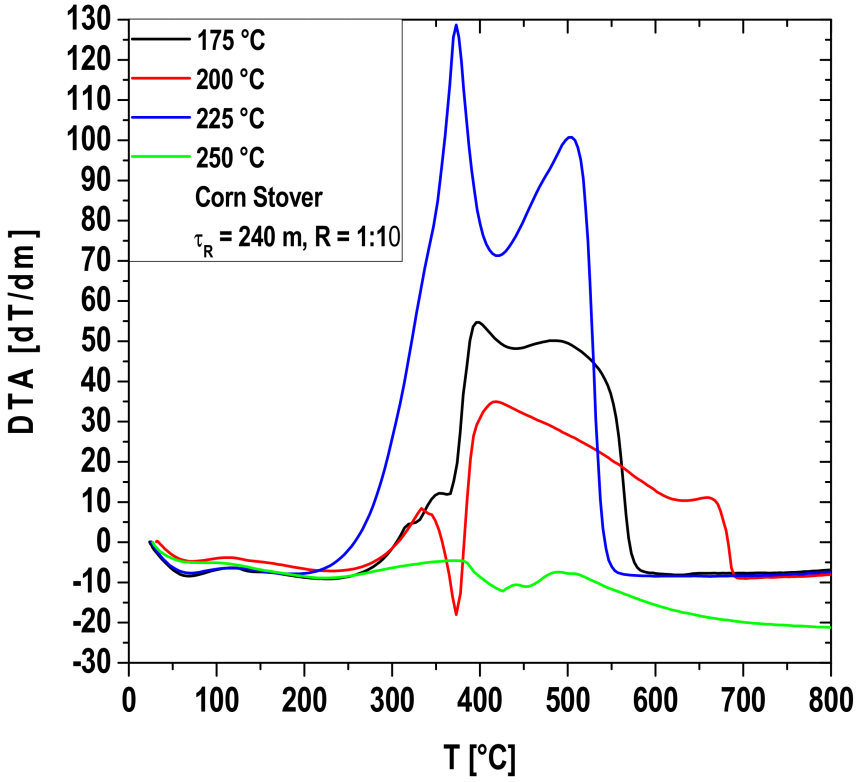

Figure 4. DTA of hydro-chars obtained by hydrothermal carbonization of corn stover at 175, 200, 225, and 250 °C, 240 min, and biomass/H_2O proportion of 1:10, using a reactor of 18.927 L.

The mass balance by hydrothermal carbonization of corn stover at 175 °C shows that approximately 63.0 (wt.%) of initial biomass still remains as solid phase reaction products [52]. In addition, the low concentration of lignin-derived reaction compounds such

as phenols and guajacol in the aqueous phase indicates that only a small portion of lignin has been thermally degraded [52]. Contrarily, the high concentration of cellulose/hemi-cellulose-derived reaction compounds in the aqueous phase including furfural, HMF, and acetic acids is a sign that higher amounts of cellulose/hemi-cellulose compared to lignin have been thermally degraded [52].

Since corn stover consist basically by cellulose + hemi-cellulose (69.0%), lignin (20.0%), ash (8.0%) [60–62], and small amounts of soluble substances [61], the TG/DTG analysis shows that almost all cellulose + hemi-cellulose and soluble substances in the aqueous phase have been thermally degraded, as well as approximately the haft of lignin, thus remaining within the solid phase reaction products the inorganic matter and lignin. In the last step, between 530 and 800 °C, a mass loss of approximately 11.0–12.0 (wt.%) occurred, associated with the thermal degradation and/or combustion of lignin. The ash content of 8.0 (wt.%) is according to that reported in the literature [60–62].

The thermal degradation of corn stover after hydrothermal processing at 200 °C shows the occurrence of 03 reaction steps. In the first one, between 25 and 110 °C, a mass loss of approximately 2.0 (wt.%) occurred, because of humidity removal, as well as the degradation of low molecular weight compounds (volatile compounds) adsorbed into the pores of solid phase products such as methanol. [6,52]. In the second degradation step, between 110 and 520 °C, a mass loss of approximately 62.0 (wt.%) was observed. The mass balance by hydrothermal carbonization of corn stover at 200 °C shows that approximately 57.4 (wt.%) of initial biomass still remains as solid phase reaction products [52]. Although, the concentrations of lignin-derived reaction compounds in process water such as phenols and guajacol has increased between 175 and 200 °C [52], still a small portion of lignin has been thermally degraded. The high concentration of cellulose/hemi-cellulose-derived reaction compounds in the aqueous phase including furfural, HMF, and acetic acids show that high amount of cellulose/hemi-cellulose has been thermally degraded [52], remaining within the solid phase reaction products the inorganic matter and lignin. In the third step, between 520 and 800 °C, a mass loss of approximately 32.0 (wt.%) occurred, associated with the thermal degradation and/or combustion of lignin. The ash content of 4.0 (wt.%) is according to that reported in the literature [60–62].

One observes, for the thermal degradation of corn stover after hydrothermal processing at 225 °C, the occurrence of 03 reaction steps. In the first one, between 25 and 130 °C, a mass loss of approximately 2.0 (wt.%) occurred, because of humidity removal, as well as the degradation of low molecular weight compounds (volatile compounds) adsorbed into the pores of solid phase products including alcohols (methanol, ethanol), volatile carboxylic acids (acetic acid, propanoic acid) [6], and aldehydes (HMF). In the second degradation step, between 130 and 530 °C, a mass loss of approximately 92.0 (wt.%) occurred. The mass balance by hydrothermal carbonization of corn stover at 225 °C shows that approximately 41.0 (wt.%) of initial biomass still remains as solid phase reaction products [52]. The high concentration of lignin-derived reaction compounds in process water such as phenols and guajacol, as well as cellulose/hemi-cellulose-derived reaction chemicals dissolved in process water such as carboxylic acid, show that most of lignin and cellulose/hemi-cellulose have been thermally degraded [52], remaining within the solid phase reaction products the inorganic matter. In the third step, between 530 and 800 °C, a mass loss of approximately 3.0 (wt.%) occurred, associated with the thermal degradation and/or combustion of lignin. The ash content of 3.0 (wt.%) is according to that reported in the literature [60–62].

The thermal degradation of corn stover after hydrothermal processing at 250 °C shows the occurrence of 04 reaction steps. In the first one, between 25 and 110 °C, a mass loss of approximately 1.0 (wt.%) occurred, due to the release of moisture. In the second degradation step, between 110 and 270 °C, a mass loss of approximately 9.0 (wt.%) has been observed. In the third degradation step, between 270 and 430 °C, a mass loss of approximately 15.0 (wt.%) occurred. In the last degradation step, between 430 and 800 °C, a mass loss of approximately 25.0 (wt.%) occurred. The mass balance by hydrothermal carbonization of corn stover at 250 °C shows that approximately 35.8 (wt.%) of initial

biomass still remains as solid phase reaction products [52]. The high concentration of cellulose/hemi-cellulose-derived reaction chemicals in process water such as acetic acid, as well as lignin-derived reaction compounds solvated in process water such as guajacol and phenols, show that high amounts of cellulose/hemi-cellulose and lignin have been thermally degraded [52], being the solid phase reaction products a carbon rich material. Finally, the results illustrated in Figures 2 and 3 are in accord to a similar study described in the literature, for the thermal analysis of corn stover, by Mohammed et al. [63].

Finally, one observes in Figure 3, for the hydro-chars obtained at 175 and 200 °C, that highest mass loss are associated with the occurrence of endothermic peaks at 355.2 and 362.9 °C, respectively. This behavior, was also observed in Figure 4 by the presence of exothermic peaks around 360 °C. For the hydro-chars obtained at 225 and 250 °C, the endothermic peaks occurred at 397 and 434 °C, respectively, showing that the higher the temperature the higher the thermal stability of solid reaction products. In addition, the hydro-char obtained at 250 °C presented the highest thermal stability compared to the hydro-chars obtained at 175, 200, and 225 °C, as it presented the lowest mass loss of 50.51% (wt.) between the temperatures of 144 and 768.5 °C.

3.1.2. SEM Analysis

The microscopic analyses of hydro-chars obtained at 175, 200, 225, and 250 °C, 240 min, and biomass/H_2O proportion of 1:10, using a reactor of 18.927 L, are illustrated in Figure 5a,b and Figure 6a,b, respectively. The SEM image in Figure 5a indicates a rigid and well-organized fiber structure, demonstrating that temperature had almost no effect on the vegetal structure, as it largely retained the original morphological microscopic characteristics. The results are in agreement to analogous investigations on the effect of process temperature over the morphology of hydro-chars produced by corn stover [63], and corn straw [64].

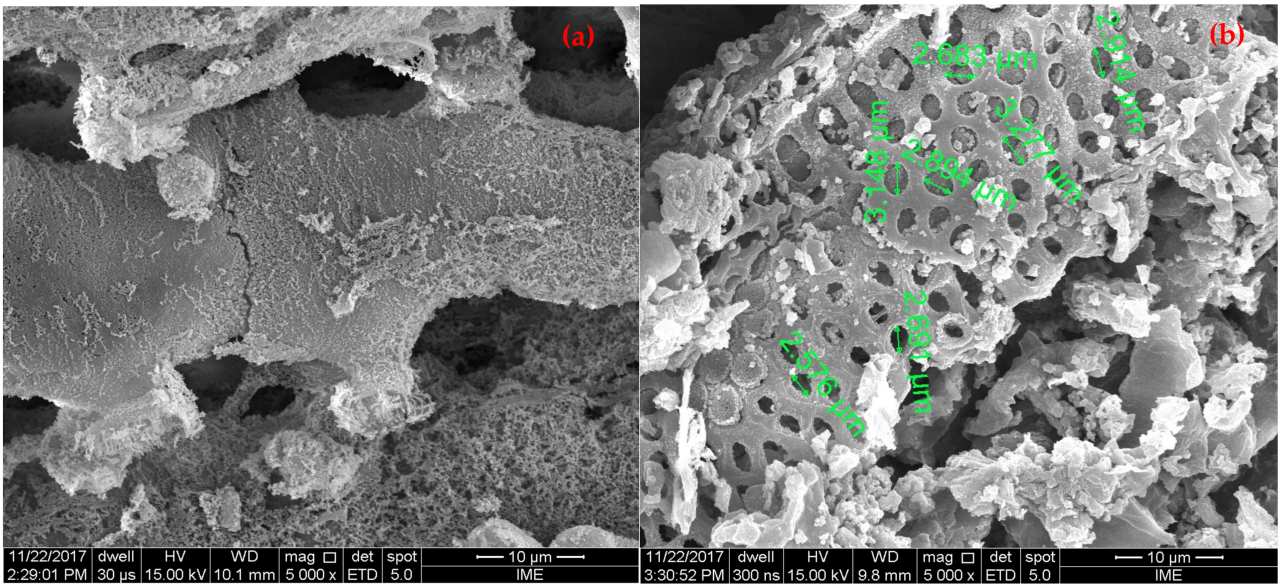

Figure 5. SEM of corn stover after hydrothermal processing at 175 °C (**a**) and 200 °C (**b**), 240 m, and biomass/H_2O proportion of 1:10, using a reactor of 18.927 L (Mag: 5000×).

The SEM image illustrated in Figure 5b shows that disaggregate, amorphous, and heterogeneous structures with nonuniform geometry dominated, demonstrating that temperature had caused the appearance of micropores with average diameter of 3.00 µm, indicating that the lignocellulose material started to decompose. However, process temperature still had little effect on the vegetal structure, as it largely retained the original microscopic characteristics. The results are in agreement to similar investigations described by Xing et al. [64], and Mohammed et al. [63].

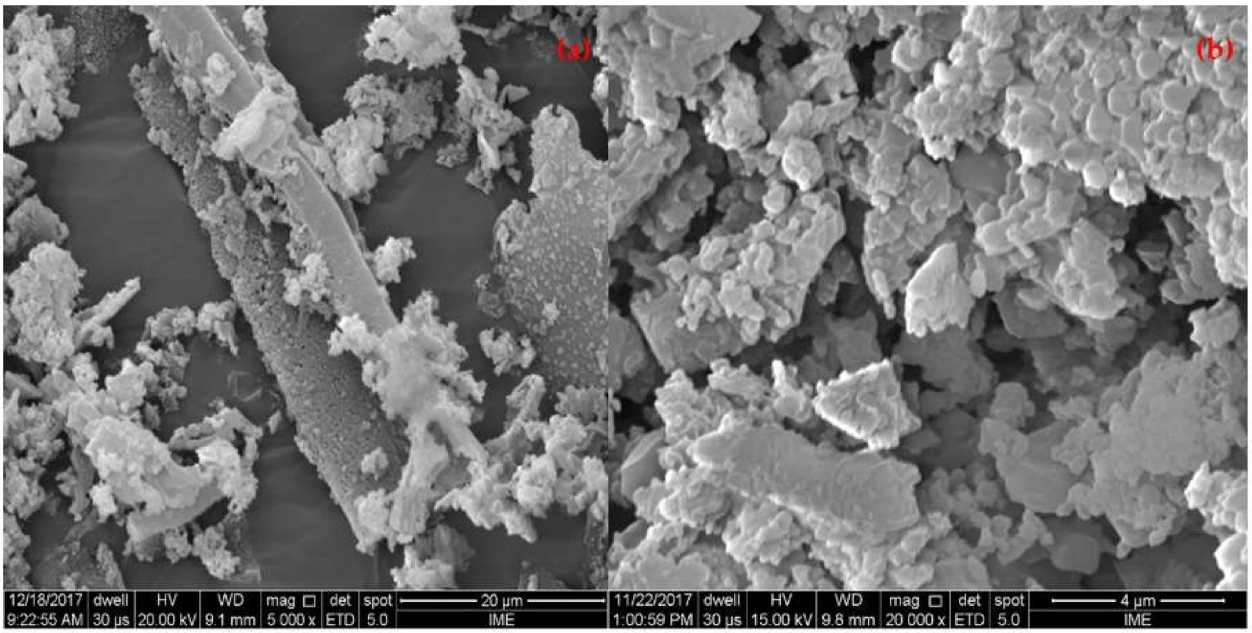

Figure 6. SEM of corn stover after hydrothermal processing at 225 °C (**a**) and 250 °C (**b**), 240 m, and biomass/H_2O proportion of 1:10, using a reactor of 18.927 L (Mag: 5000×).

The SEM image in Figure 6a indicates that hydro-char structure consists of agglomerated micro-spheres and heterogeneous structures with irregular shapes (fragmentation), showing particle size averaging 0.5 µm as depicted in detail by Figures S1 and S2 in Supplementary Materials. The agglomerated micro-spheres and fragmentation indicates that cellulose and hemi-cellulose were decomposed, as reported by Xing et al. [64], demonstrating that temperature had generated significant alterations on the morphological structure of corn stover by destructing the plant cell walls [6]. Xing et al. [64] reported the occurrence of micro-spheres by the hydrothermal carbonization of corn straw at 230 °C, 30 min, and biomass/H_2O proportion of 1:8.

One observes in Figure 6b an aggregate amorphous solid phase consisting of microspheres and heterogeneous structures with nonuniform geometry (fragmentation), showing that original vegetal surface structure had been drastic changed, and was the carbonization grade higher compared to the SEM image at 225 °C. In fact, process temperature had generated significant alterations on the morphological structure of corn stover by destructing the plant cell structure. The agglomerated micro-spheres and fragmentation indicates that cellulose and hemi-cellulose were decomposed. Xing et al. [64] reported the occurrence of a similar structure by the hydrothermal carbonization of corn straw at 260 °C, 30 min, and biomass/H2O proportion of 1:8.

3.1.3. EDX Analysis

Table 1 shows the EDX (energy dispersive X-ray spectroscopy) analysis of hydro-chars. The samples were analyzed at five different points. By increasing the temperature, the carbon content increased and that of oxygen diminished. By comparing the results for the carbon content in Table 1 and those described in Supplementary Table S1, one observes that the EDX technique exhibited higher carbon contents but similar oxygen contents. This was probably due to limitations of the technique, as it was not adequate to identify/recognize elements such as nitrogen and hydrogen. In addition, calculation of oxygen and carbon contents, described in Table S1, was computed by subtracting the ash content [52]. In addition, Ca, Zn, Cu, Mo, Na, and P, as well as Si were identified in almost all the points marked by EDX. The inorganics identified in hydro-chars by EDX in hydro-chars are in agreement to those identified in corn stover after drying at 105 °C [65]. Finally, Table 1 shows an increase on carbon content (carbonization) with increasing process temperature.

Table 1. Percentages in mass and atomic mass of hydro-chars, obtained by hydrothermal carbonization of corn stover at 175, 200, 225, and 250 °C, 240 min, biomass/H2O proportion of 1:10, using a reactor of 18.927 L, at the point marked by EDX technique [6].

Hydro-Chars												
	175 °C			200 °C			225 °C			250 °C		
Chemical Elements	Mass (wt.%)	Atomic Mass (wt.%)	SD	Mass (wt.%)	Atomic Mass (wt.%)	SD	Mass (wt.%)	Atomic Mass (wt.%)	SD	Mass (wt.%)	Atomic Mass (wt.%)	SD
C	60.69	67.56	0.503	71.98	77.43	0.818	73.89	79.17	0.654	76.04	81.05	0.631
O	38.57	32.24	0.504	27.83	22.47	0.819	25.73	20.70	0.656	23.59	18.87	0.632
Si	0.136	0.065	0.020	0.194	0.089	0.043	-	-	-	-	-	-
Ca	0.181	0.061	0.018	-	-	-	0.374	0.120	0.032	-	-	-
Zn	-	-	-	-	-	-	-	-	-	0.366	0.072	0.065
Cu	0.210	0.044	0.042	-	-	-	-	-	-	-	-	-

SD = standard deviation.

3.1.4. XRD Analysis

The XRD (X-ray diffraction) data of hydro-chars obtained by hydrothermal processing of corn stover at 175, 200, 225, and 250 °C, 240 min, and biomass/H_2O proportion of 1:10, using a reactor of 18.927 L, is illustrated in Figure 7a,b and Figure 8a,b, respectively.

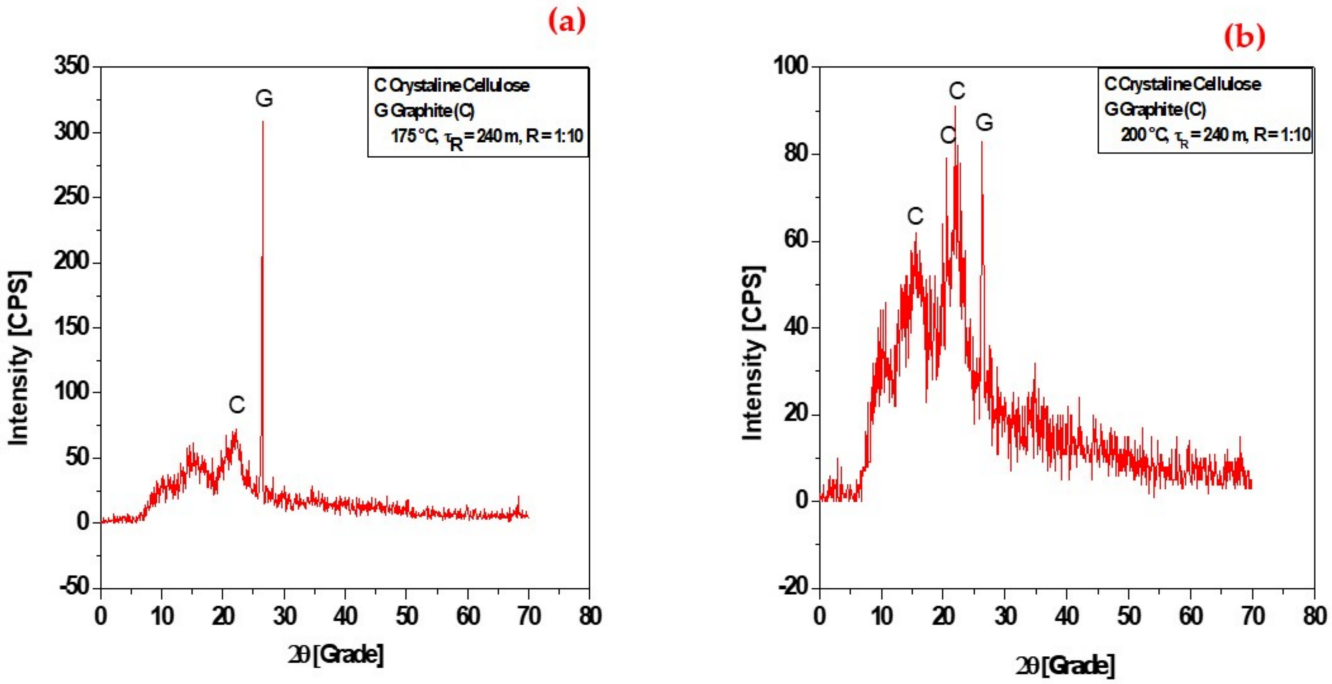

Figure 7. XRD of hydro-chars obtained by hydrothermal carbonization of corn stover at 175 °C (**a**) and 200 °C (**b**), 240 min, and biomass/H_2O proportion of 1:10, using a reactor of 18.927 L.

The diffractogram of corn stover obtained by hydrothermal carbonization at 175 °C, is illustrated in Figure 7a. It shows the presence of two crystalline phases—graphite (C) with a peak of higher intensity (100%) on the position 2θ: 26.47, and crystalline cellulose with a peak of higher intensity (12.95%) on the position 2θ: 22.20. The peak on the position 2θ: 22.20 is characteristics of crystalline cellulose structure, as described by Regmi et al. [5] and Kang et al. [66], who identified diffraction peaks on the positions 2θ: 15.3 and 22.3 [5,66].

At 200 °C, X-ray-diffraction data identified two crystalline phases—crystalline cellulose with a peak of higher intensity (100%) on the positions 2θ: 20.68, 15.53 (79%), and 21.96 (90.07%), because of amorphous cellulose matrix degradation and the exposure of

the crystalline cellulose [57], and graphite (C) with a peak of medium intensity (59.38%) on the position 2θ: 26.45, as shown in Figure 7b.

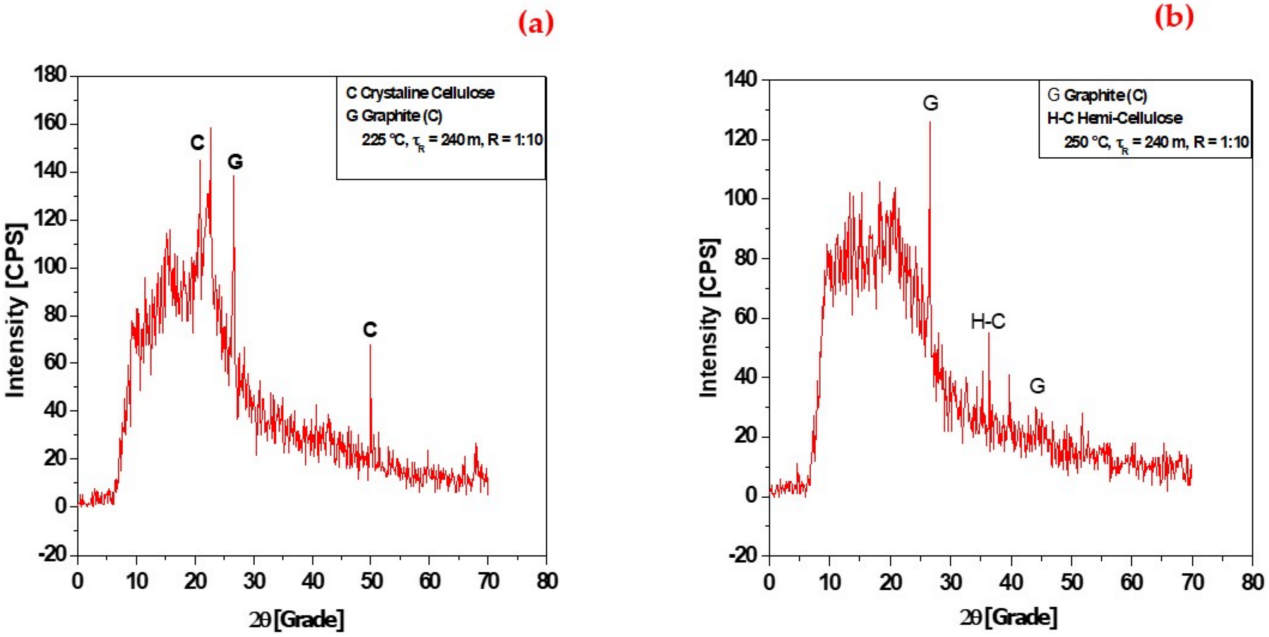

Figure 8. XRD of hydro-chars obtained by hydrothermal carbonization of corn stover at 225 °C (**a**) and 250 °C (**b**), 240 min, and biomass/H_2O proportion of 1:10, using a reactor of 18.927 L.

The XRD at 225 °C identified two crystalline phases—graphite (C) with a peak of medium intensity (53.75%) on the position 2θ: 26.57, and crystalline cellulose with peaks of high and low intensity on the positions 2θ: 22.47 (100%) and 49.94 (49.86%), as well as three peaks of medium and low intensity on the positions 2θ: 20.73 (65.99%) and 49.94 (49.86%), as shown in Figure 8a.

The diffractograms (XRD) identified the occurrence of peaks of higher intensity of graphite (C) as the temperature increased, as well as a decrease of peaks intensity for crystalline cellulose, demonstrating that higher temperatures favor the formation of crystalline-phase graphite (C), being in agreement to the results illustrated in Table 1.

3.1.5. BET

Figure 9 shows the BET analysis of hydro-char obtained by HTC of corn stover at 250 °C, 240 min, and biomass/H_2O of 1:10, using a reactor of 18.927 L. The N_2 capacity increased as the relation (P/P_0) increased, showing a maximum capacity of approximately 12 cm^2/g as the relative pressure approached 1.0. The density of hydro-char was 2.10 g/cm^3, and the surface area measured by relative pressure (P/P_0 = 0.201) was 4.02 m^2/g, while the surface area was 4.3498 m^2/g. The pore volume measured by reduced pressure (P/P_0 = 0.988) was 0.01857 cm^3/g. The average pore width was 17.079 μm.

3.2. Adsorption Kinetics of Acetic Acid (CH_3COOH) on Hydro-Char

One of the great disadvantages of hydrothermal processing of lignocellulose-rich materials, such as biomass, is the occurrence of hazardous lignin and cellulose-derived reaction products including phenols, furfural, and hydroxymethylfurfural in the aqueous phase [52–55,67,68]. In addition, the high concentration of carboxylic acids (acetic acid, propionic acid, etc.), in process water confers its high acidity [52–55,68,69]. From this perspective, the hydro-char obtained by HTC at 250 °C, 240 min, biomass/H_2O proportion of 1:10, was chemically activated with alkali (2.0 M NaOH) and acid (2.0 M HCl) solutions in order to investigate the its capacity to selectively uptake (adsorb) acetic acid from

model aqueous solutions (1.0, 2.0, 3.0, and 4.0 mg/mL), the major carboxylic acid within hydrothermal carbonization process water streams.

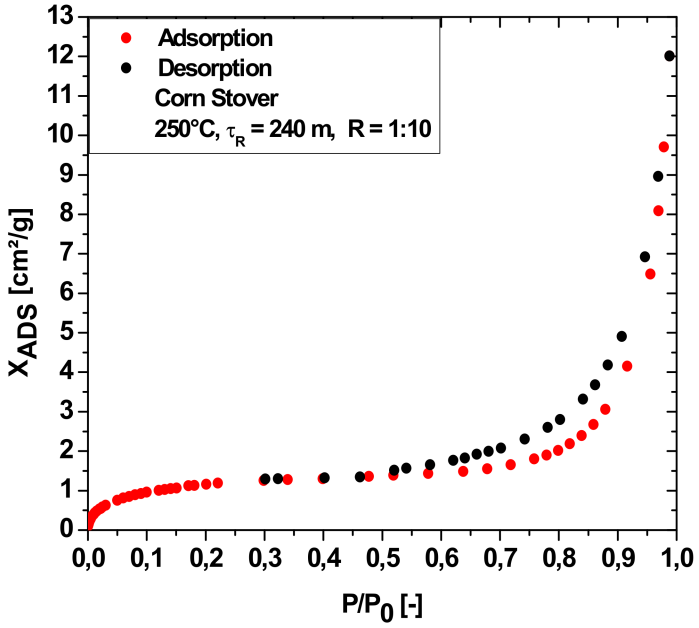

Figure 9. BET of hydro-char obtained by hydrothermal carbonization of corn stover at 250 °C, 240 min, and biomass/H_2O of 1:10, using a reactor of 18.927 L.

3.2.1. Bio-Adsorbent Activation with NaOH

Influence of Acetic Acid Concentration

Figure 10 illustrates the influence of acetic acid initial solution concentration (2.0, 3.0, and 4.0 mg mL^{-1}) on the adsorption kinetics within hydro-char produced by HTC at 250 °C, 240 min, biomass/H_2O proportion of 1:10, alkali-activated (2.0 M NaOH), 0.1 $g_{Adsorbent}$/10 $mL_{CH3COOH}$. The adsorption kinetic is rapid and equilibrium is reached between 240 and 480 s. The activation of hydro-char with a strong alkali such as NaOH causes significant changes in the surface and porous (micropores, mesopores, and macropores) structure [8,9]. The acetic acid molecules solvated in H_2O are selectively caught by the negative-charged active sites, which is according to Liang et al. [69], who reported that adsorption process of CH_3COOH on carbon microspheres, prepared by hydrothermal carbonization of starch, was mainly due to the porous (micropores, mesopores, and macropores) structure transformations caused by destruction of hydrophilic oxygen functional groups. In addition, Liang et al. [69] proved that pore structure determines the adsorption capacity and diffusion rate and the process is physical.

The absorption of acetic acid molecules occurs because of a concentration difference between the solution and hydro-char surface and internal porous, micro-porous, and macroporous structure, as well as the appearance of dipole–dipole electrostatic attraction forces between the negative charged sites within the porous and the dissociated H^+ of R-COOH (H^+ + R-COO^-). The adsorption kinetic data of acetic acid on hydro-char was correlated with a first order model, exhibiting *root-mean-square error* (r^2) between 0.969 and 0.999, as shown in Table 2, which is in agreement with the results described by Machado et al. [6]. It can be also observed that dimensionless acid value I(τ), increases with decreasing acetic acid solutions concentrations (2.0, 3.0, and 4.0 mg mL^{-1}), that is, the lower the acetic acid solution concentration, the higher the adsorption efficiency.

The influence of acetic acid initial solution concentration (1.0, and 2.0 mg mL^{-1}) on the adsorption kinetics within hydro-char obtained by hydrothermal processing of corn stover at 250 °C, 240 min, biomass/H_2O proportion of 1:10, chemically activated with

NaOH (2.0 M), 0.2 $g_{Adsorbent}$/10 $mL_{CH3COOH}$, is illustrated in Figure 11. One can observe that dimensionless acid value I(τ), increases with decreasing CH_3COOH concentrations (1.0, and 2.0 mg/mL), that is, the lower the acetic acid solution concentration, the higher the adsorption efficiency. In addition, by comparing Figures 10 and 11, it is easy to observe that higher adsorbent-to-solution ratios favors the adsorption efficiency, due to an increase on the surface area. The adsorption kinetic data of acetic acid on hydro-char was correlated with a first order model, exhibiting root-mean-square error (r^2) between 0.969 and 0.982, as shown in Table 3.

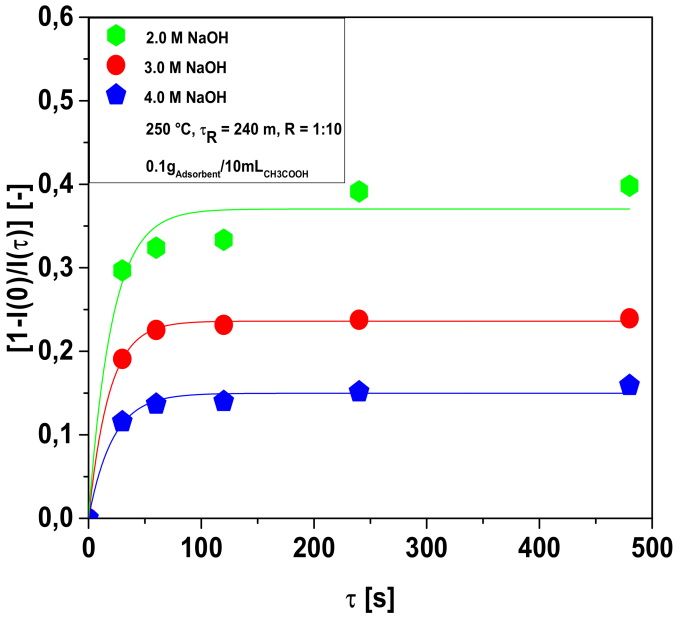

Figure 10. Adsorption kinetic of CH_3COOH solutions, expressed as dimensionless acid value I(τ), on NaOH-activated hydro-char obtained at 250 °C.

Table 2. Regression parameters by adsorption kinetic of CH_3COOH solutions (2.0, 3.0, and 4.0 mg mL^{-1}), expressed as dimensionless acid value, on NaOH (2.0 M)-activated hydro-char produced by hydrothermal processing of corn stover at 250 °C, 240 min, and biomass/H_2O proportion of 1:10, 0.1 $g_{Adsorbent}$/10 $mL_{CH3COOH}$.

Parameters	$C_{CH3COOH}$ (mg/mL)		
	2	3	4
Pseudo-first-order			
$I^{L}_{CHeCOOH}(0)$ (-)	0.3694	0.2361	0.1497
κ (s^{-1})	0.0479	0.0545	0.0468
r^2	0.969	0.999	0.988

Influence of Adsorbent-to-Solution Ratio

The effect of hydro-char/solution ratio on the adsorption kinetics of acetic acid solution (2.0 mg mL^{-1}) within NaOH (2.0 M)-activated hydro-char obtained by hydrothermal processing of corn stover at 250 °C, 240 min, biomass/H_2O proportion of 1:10, is illustrated in Figure 12. The adsorption performance increased with increasing hydro-char/solution ratio increase as the number of active sites on surface and porous (micropores, mesopores, and macropores) structure increased, that is, by increasing the hydro-char/solution ratio, the surface area increased. The adsorption kinetic data of acetic acid on hydro-char was correlated with a first order model, exhibiting root-mean-square error (r^2) between 0.973 and 0.982, as shown in Table 4.

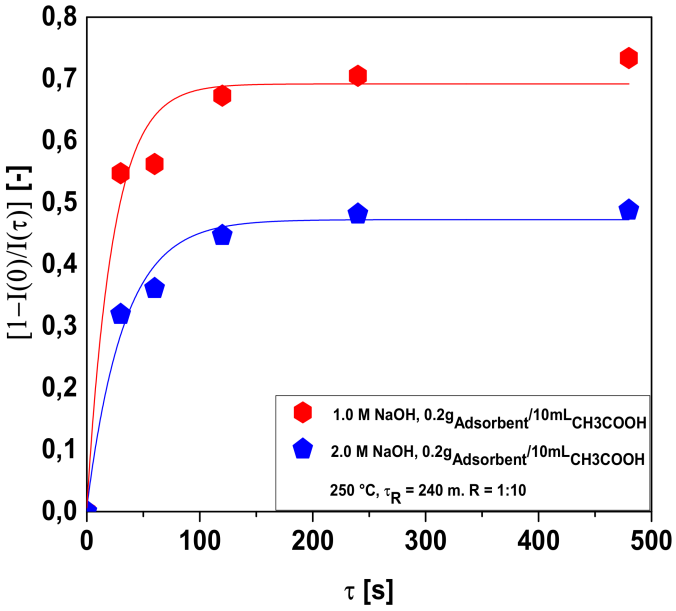

Figure 11. Adsorption kinetic of CH_3COOH solutions (1.0 and 2.0 mg mL^{-1}), expressed as dimensionless acid value I(τ), on NaOH (2.0 M)-activated hydro-char produced by hydrothermal processing of corn stover at 250 °C, 240 min, and biomass/H_2O proportion of 1:10, 0.2 $g_{Adsorbent}/10$ $mL_{CH3COOH}$.

Table 3. Regression parameters by adsorption kinetic of CH_3COOH solutions (1.0 and 2.0 mg mL^{-1}), expressed as dimensionless acid value, on NaOH (2.0 M)-activated hydro-char produced by hydrothermal processing of corn stover at 250 °C, 240 min, and biomass/H_2O proportion of 1:10, 0.2 $g_{Adsorbent}/10$ $mL_{CH3COOH}$.

Parameters	$C_{CH3COOH}$ (mg/mL)	
	1	2
Pseudo-first-order		
$I^{L}_{CHeCOOH}(0)$ (-)	0.4689	0.3694
κ (s^{-1})	0.0305	0.0479
r^2	0.982	0.969

Table 4. Regression parameters by the effect of hydro-char/solution ratio (0.1 $g_{Adsorbent}/10$ $mL_{CH3COOH}$, 0.2 $g_{Adsorbent}/10$ $mL_{CH3COOH}$) on adsorption kinetic of CH_3COOH, expressed as dimensionless acid value I(τ), on NaOH (2.0 M)-activated hydro-char produced by hydrothermal processing of corn stover at 250 °C, 240 min, and biomass/H_2O proportion of 1:10.

Parameters	$C_{CH3COOH}$ (mg/mL)	
	2	2
Pseudo-first-order	0.1 $g_{Adsorbent}/10$ $mL_{CH3COOH}$	0.2 $g_{Adsorbent}/10$ $mL_{CH3COOH}$
$I^{L}_{CHeCOOH}(0)$ (-)	0.4689	0.6889
κ (s^{-1})	0.0305	0.0430
r^2	0.982	0.973

3.2.2. Bio-Adsorbent Activation with HCl

Influence of Hydrochloric Acid Concentration

The influence of acetic acid initial solution concentration (1.0, 2.0, 3.0, and 4.0 mg mL^{-1}) on the adsorption kinetics within HCl (2.0 M)-activated hydro-char obtained by on hydro-char obtained by hydrothermal processing of corn stover at 250 °C, 240 min, biomass/H_2O proportion of 1:10, 0.2 $g_{Adsorbent}/10$ $mL_{CH3COOH}$, is shown in Figure 13.

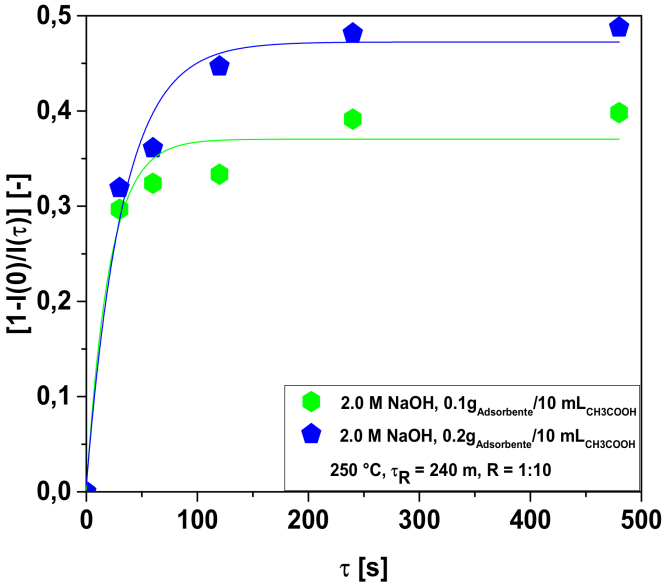

Figure 12. Effect of hydro-char/solution ratio (0.1 $g_{Adsorbent}$/10 $mL_{CH3COOH}$, 0.2 $g_{Adsorbent}$/10 $mL_{CH3COOH}$) on adsorption kinetic of CH_3COOH, expressed as dimensionless acid value I(τ), on NaOH (2.0 M)-activated hydro-char produced by hydrothermal processing of corn stover at 250 °C, 240 min, and biomass/H_2O proportion of 1:10.

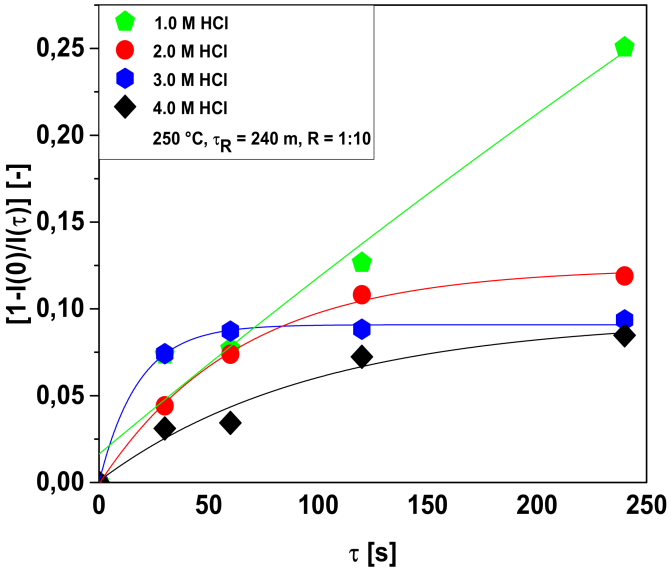

Figure 13. Adsorption kinetic of CH_3COOH solutions (1.0, 2.0, 3.0, and 2.0 mg mL^{-1}), expressed as dimensionless acid value I(τ), on HCl (2.0 M)-activated hydro-char produced by hydrothermal processing of corn stover at 250 °C, 240 min, and biomass/H_2O proportion of 1:10, 0.1 $g_{Adsorbent}$/10 $mL_{CH3COOH}$.

The adsorption kinetic was rapid and equilibrium was reached around 240 s. The activation of hydro-char with a strong acid such as HCl causes significant changes and/or damages on the surface and porous (micropores, mesopores, and macropores) structure [51]. The acetic acid molecules solvated/dissociated in water are not efficiently captured by the positive charged active sites. The absorption of acetic acid molecules is due basically to a concentration difference between bulk solution and hydro-char surface and porous (micropores, mesopores, and macropores) structure, as the positive-charged sites on the surface and within the internal porous structure contribute to the appearance of electrostatic repulsion forces between the dissociated H^+ of R-COOH (H^+ + R-COO^-) and the positive

charged sites. This is according to Liang et al. [69], who proved that pore structure determines the adsorbent capacity and that process is diffusion-rate controlled. The adsorption kinetic data of acetic acid on hydro-char was correlated with a first order model, exhibiting root-mean-square error (r^2) between 0.967 and 0.997, as shown in Table 5.

Table 5. Regression parameters by adsorption kinetic of CH_3COOH solutions (1.0, 2.0, 3.0, and 4.0 mg mL^{-1}), expressed as dimensionless acid value I(t), on HCl (2.0 M) hydro-char produced by HTC of corn stover at 250 °C, 240 min, and biomass/H_2O proportion of 1:10, 0.1 $g_{Adsorbent}$/10 $mL_{CH3COOH}$.

Parameters	$C_{CH3COOH}$ (mg/mL)			
	1	**2**	**3**	**4**
Pseudo-first-order				
$I^{L}_{CHeCOOH}(0)$ (-)	-	0.1241	0.0908	0.0941
κ (s^{-1})	-	0.0156	0.0563	0.0101
r^2	0.969	0.998	0.978	0.967

The results presented in Figures 10 and 13 show that NaOH (2.0 M) chemically activated hydro-char is not only more efficient than that activated with HCl (2.0 M), but also presents the highest adsorption performance and capacity.

3.2.3. Adsorption Equilibrium Isotherms of Acetic Acid (CH_3COOH) on Hydro-Char

The Langmuir isotherm was applied to correlate the equilibrium adsorption data of CH_3COOH on alkali (2.0 M NaOH)- and acid (2.0 M HCl)-activated hydro-char produced by hydrothermal processing of corn stover at 250 °C, 240 min, biomass/H2O proportion of 1:10, 0.1 $g_{Adsorbent}$/10 $mL_{CH3COOH}$, as illustrated by Figure 14.

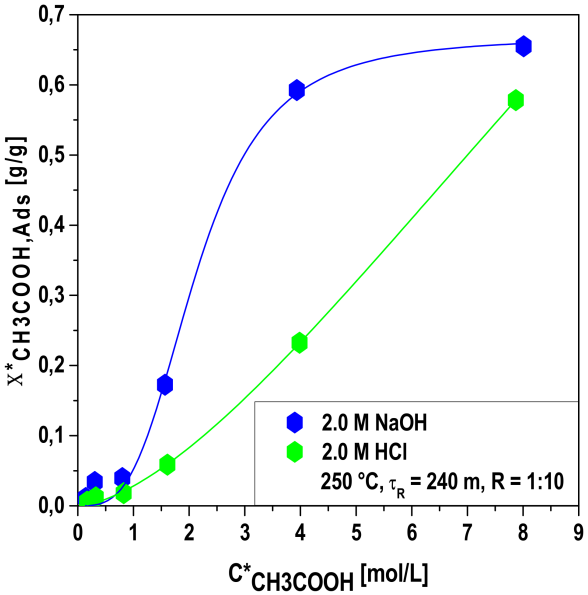

Figure 14. Langmuir adsorption isotherm of CH_3COOH solutions (0.5, 0.25, 0.1, 0.05, 0.02, and 0.01 M) within NaOH (2.0 M)- and HCl (2.0 M)-activated hydro-chars produced by hydrothermal carbonization of corn stover at 250 °C, 240 min, and biomass/H_2O proportion of 1:10.

The adsorption isotherm of acetic acid on NaOH- and HCl-activated hydro-char was correlated with the Langmuir model, exhibiting root-mean-square errors (r^2) of 0.994 and 0.989, respectively. The equilibrium adsorbent-phase concentration of CH_3COOH for NaOH- and HCl-activated hydro-chars were approximately 650 and 575 mg/g, respectively. The bio-adsorbent (hydro-chars) equilibrium loadings were in agreement

with the adsorption of MB (methylene blue) from aqueous solution on NaOH-activated hydro-chars produced by HTC of factory-rejected tea and palm date seeds, as reported by Islam et al. [8,9], correlated using a pseudo-second-order model and the adsorption isotherms by the Langmuir [8], and the Freundlich models [9], respectively. For the adsorption kinetic of MB (methylene blue) on NaOH-activated hydro-chars produced by HTC of from factory-rejected tea and palm date seeds, maximum adsorption loadings of 487.4 mg/g at 30 °C [8], and 612.1, 464.3, and 410.0 mg/g at 30, 40, and 50 °C [9], were reported, respectively. Finally, the adsorption of CH_3COOH on carbon microspheres synthesized by hydrothermal carbonization was investigated by Liang et al. [69], reporting equilibrium adsorbent-phase concentration of CH_3COOH of 260 mg/g at 25 °C.

4. Conclusions

TG/DTG analysis showed, for the hydro-chars obtained at 175 and 200 °C, that highest mass loss was associated with the occurrence of endothermic peaks at 355.2 and 362.9 °C, respectively. This was also confirmed by DTA analysis by the presence of exothermic peaks around 360 °C. For the hydro-chars obtained at 225 and 250 °C, the endothermic peaks occurred at 397 and 434 °C, respectively, showing that the higher the temperature the higher the thermal stability of solid reaction products. The hydro-char obtained at 250 °C presented the highest thermal stability compared to the hydro-chars obtained at 175, 200, and 225 °C, as it presented the lowest mass loss of 50.51% (wt.) between the temperatures 144 and 768.5 °C.

SEM images indicate a rigid and well-organized fiber structure by hydrothermal processing of corn stover at 175 and 200 °C, demonstrating that temperature had almost no effect on the vegetal structure, as it largely retained the original morphological microscopic characteristics. On the other hand, SEM images of hydro-char produced by hydrothermal carbonization of corn stover at 225 and 250 °C indicate that hydro-char structure consisted of agglomerated micro-spheres and heterogeneous structures with irregular shapes (fragmentation). The agglomerated micro-spheres and fragmentation indicates that cellulose and hemi-cellulose were decomposed, as reported by Xing et al. [62], demonstrating that temperature had generated significant alterations on the morphological structure of corn stover by destructing the plant cell structure/walls [6].

As observed by EDX analysis, by increasing the temperature, the carbon content increased and that of oxygen diminished. The diffractograms (XRD) identified the occurrence of peaks of higher intensity of graphite (C) as the temperature increased, demonstrating that higher temperatures favors the formation of crystalline-phase graphite (C).

The analysis of acetic acid adsorption kinetics data, the main volatile carboxylic acid identified in the hydrothermal carbonization liquid phase, showed that NaOH (2.0 M)-activated hydro-char obtained by hydrothermal processing of corn stover at 250 °C, 240 min, biomass/H_2O proportion of 1:10, presented the highest adsorption performance and capacity. The chemically activated hydro-chars were selective to uptake of CH_3COOH, demonstrating that enriching/recovery of CH_3COOH from HTC process water streams is possible.

Supplementary Materials: The following are available online at https://www.mdpi.com/article/10.3390/en14238154/s1, Figure S1: SEM of corn stover after hydrothermal processing at 225 °C, 240 min, and biomass/H_2O ratio of 1:10, using a reactor of 18,927 L (Mag: 30,000×). Figure S2: SEM of corn stover after hydrothermal processing at 225 °C, 240 min, and biomass/H_2O ratio of 1:10, using a reactor of 18.927 L (Mag: 30,000×). Table S1: Physical chemistry and elemental analysis of corn stover after hydrothermal processing at 175, 200, 225, and 250 °C, 240 min, and biomass/H_2O ratio of 1:10, using a reactor of 18.927 l. (MM = moist matter, TS = total solids.) [52].

Author Contributions: The individual contributions of all the co-authors are provided as follows: M.E.G.C. contributed to the methodology, formal analysis, and writing of the original draft paper; M.C.S. contributed to the formal analysis, methodology, and software; L.M.P. contributed to the formal analysis and software; F.P.d.C.A. contributed to the formal analysis and software; T.T. contributed to the formal analysis and software; C.E.F.d.C. contributed to the chemical analysis;

M.S. contributed to the investigation, methodology, and chemical analysis; T.H. contributed to the resources and infrastructure; D.A.R.d.C. to the methodology, formal analysis, and co-supervision; and N.T.M. contributed to the supervision, conceptualization, and data curation. All authors have read and agreed to the published version of the manuscript.

Funding: This research was partially funded by CNPq-Brazil, grant number: 207325/2014-6.

Institutional Review Board Statement: Not applicable.

Informed Consent Statement: Not applicable.

Acknowledgments: I would like to acknowledge and dedicate this research in memory to Hélio da Silva Almeida, Professor at the Faculty of Sanitary and Environmental Engineering/UFPa, who passed away in 13 March 2021. His contagious joy, dedication, intelligence, honesty, seriousness, and kindness will always be remembered in our hearts.

Conflicts of Interest: The authors declare no conflict of interest.

Abbreviations

HTC	Hydrothermal carbonization
SEM	Scanning electron microscopy
TG/DTG/DTA	Thermogravimetric analysis
EDX	Energy dispersive X-ray spectroscopy
XRD	X-ray diffraction
BET	Surface area and pore size distribution analysis
AAEMs	Alkaline and alkaline earth metals
HMF	Hydroxymethylfurfural
CH_3COOH	Acetic acid

References

1. Kumar, S.; A Loganathan, V.; Gupta, R.B.; Barnett, M.O. An Assessment of U(VI) removal from groundwater using biochar produced from hydrothermal carbonization. *J. Environ. Manag.* **2011**, *92*, 2504–2512. [CrossRef]
2. Elaigwu, S.E.; Rocher, V.; Kyriakou, G.; Greenway, G.M. Removal of Pb2+ and Cd2+ from aqueous solution using chars from pyrolysis and microwave-assisted hydrothermal carbonization of Prosopis Africana shell. *J. Ind. Eng. Chem.* **2014**, *20*, 3467–3473. [CrossRef]
3. Liu, Z.; Zhang, F.-S. Removal of lead from water using biochars prepared from hydrothermal liquefaction of biomass. *J. Hazard. Mater.* **2009**, *167*, 933–939. [CrossRef]
4. Xue, Y.; Gao, B.; Yao, Y.; Inyang, M.; Zhang, M.; Zimmerman, A.; Ro, K.S. Hydrogen peroxide modification enhances the ability of biochar (hydrochar) produced from hydrothermal carbonization of peanut hull to remove aqueous heavy metals: Batch and column tests. *Chem. Eng. J.* **2012**, *200–202*, 673–680. [CrossRef]
5. Regmi, P.; Moscoso, J.L.G.; Kumar, S.; Cao, X.; Mao, J.; Schafran, G. Removal of copper and cadmium from aqueous solution using switchgrass biochar produced via hydrothermal carbonization process. *J. Environ. Manag.* **2012**, *109*, 61–69. [CrossRef]
6. Machado, N.; Castro, D.; Queiroz, L.; Santos, M.; Costa, C. Production and Characterization of Energy Materials with Adsorbent Properties by Hydrothermal Processing of Corn Stover with Subcritical H_2O. *J. Appl. Solut. Chem. Model.* **2016**, *5*, 117–130. [CrossRef]
7. Libra, J.; Ro, K.; Kammann, C.; Funke, A.; Berge, N.D.; Neubauer, Y.; Titirici, M.; Fühner, C.; Bens, O.; Kern, J.; et al. Hydrothermal carbonization of biomass residuals: A comparative review of the chemistry, processes and applications of wet and dry pyrolysis. *Biofuels* **2011**, *2*, 71–106. [CrossRef]
8. Islam, A.; Benhouria, A.; Asif, M.; Hameed, B.H. Methylene blue adsorption on factory-rejected tea activated carbon prepared by conjunction of hydrothermal carbonization and sodium hydroxide activation processes. *J. Taiwan Inst. Chem. Eng.* **2015**, *52*, 57–64. [CrossRef]
9. Islam, A.; Tan, I.A.W.; Benhouria, A.; Asif, M.; Hameed, B.H. Mesoporous and adsorptive properties of palm date seed activated carbon prepared via sequential hydrothermal carbonization and sodium hydroxide activation. *Chem. Eng. J.* **2015**, *270*, 187–195. [CrossRef]
10. Sun, K.; Tang, J.; Gong, Y.; Zhang, H. Characterization of potassium hydroxide (KOH) modified hydrochars from different feedstocks for enhanced removal of heavy metals from water. *Environ. Sci. Pollut. Res.* **2015**, *22*, 16640–16651. [CrossRef]
11. Li, Y.; Meas, A.; Shan, S.; Yang, R.; Gai, X. Production and optimization of bamboo hydrochars for adsorption of Congo red and 2-naphthol. *Bioresour. Technol.* **2016**, *207*, 379–386. [CrossRef]
12. Han, L.; Ro, K.S.; Sun, K.; Sun, H.; Wang, Z.; Libra, J.A.; Xing, B. New evidence for high sorption capacity of hydrochar for hydrophobic organic pollutants. *Environ. Sci. Technol.* **2016**, *50*, 13274–13282. [CrossRef]

13. Han, L.; Sun, H.; Ro, K.; Sun, K.; Libra, J.; Xing, B. Removal of antimony (III) and cadmium (II) from aqueous solution using animal manure-derived hydrochars and pyrochars. *Bioresour. Technol.* **2017**, *234*, 77–85. [CrossRef]
14. Pellera, F.-M.; Giannis, A.; Kalderis, D.; Anastasiadou, K.; Stegmann, R.; Wang, J.-Y.; Gidarakos, E. Adsorption of Cu(II) ions from aqueous solutions on biochars prepared from agricultural by-products. *J. Environ. Manag.* **2012**, *96*, 35–42. [CrossRef]
15. Zhou, N.; Chen, H.; Xi, J.; Yao, D.; Zhou, Z.; Tian, Y.; Lu, X. Biochars with excellent Pb(II) adsorption property produced from fresh and dehydrated banana peels via hydrothermal carbonization. *Bioresour. Technol.* **2017**, *232*, 204–210. [CrossRef]
16. Kirschhöfer, F.; Sahin, O.; Becker, G.C.; Meffert, F.; Nusser, M.; Anderer, G.; Kusche, S.; Klaeusli, T.; Kruse, A.; Brenner-Weiss, G. Wastewater treatment-adsorption of organic micropollutants on activated HTC-carbon derived from sewage sludge. *Water Sci. Technol.* **2015**, *73*, 607–616. [CrossRef]
17. Koottatep, T.; Fakkaew, K.; Tajai, N.; Polprasert, C. Isotherm models and kinetics of copper adsorption by using hydrochar produced from hydrothermal carbonization of faecal sludge. *J. Water, Sanit. Hyg. Dev.* **2017**, *7*, 102–110. [CrossRef]
18. Sun, K.; Gao, B.; Ro, K.; Novak, J.M.; Wang, Z.; Herbert, S.; Xing, B. Assessment of herbicide sorption by biochars and organic matter associated with soil and sediment. *Environ. Pollut.* **2012**, *163*, 167–173. [CrossRef]
19. Eibisch, N.; Schroll, R.; Fuß, R.; Mikutta, R.; Helfrich, M.; Flessa, H. Pyrochars and hydrochars differently alter the sorption of the herbicide isoproturon in an agricultural soil. *Chemosphere* **2015**, *119*, 155–162. [CrossRef]
20. Zhu, X.; Liu, Y.; Zhou, C.; Luo, G.; Zhang, S.; Chen, J. A novel porous carbon derived from hydrothermal carbon for efficient adsorption of tetracycline. *Carbon* **2014**, *77*, 627–636. [CrossRef]
21. Fernandez, M.E.; Ledesma, B.; Román, S.; Bonelli, P.R.; Cukierman, A.L. Development and characterization of activated hydrochars from orange peels as potential adsorbents for emerging organic contaminants. *Bioresour. Technol.* **2015**, *183*, 221–228. [CrossRef]
22. Sun, K.; Ro, K.; Guo, M.; Novak, J.; Mashayekhi, H.; Xing, B. Sorption of bisphenol A, 17α-ethinyl estradiol and phenanthrene on thermally and hydrothermally produced biochars. *Bioresour. Technol.* **2011**, *102*, 5757–5763. [CrossRef]
23. Fang, J.; Gao, B.; Chen, J.; Zimmerman, A.R. Hydrochars derived from plant biomass under various conditions: Characteri-zation and potential applications and impacts. *Chem. Eng. J.* **2015**, *267*, 253–259. [CrossRef]
24. Fang, J.; Gao, B.; Zimmerman, A.R.; Ro, K.S.; Chen, J. Physically (CO2) activated hydrochars from hickory and peanut hull: Preparation, characterization, and sorption of methylene blue, lead, copper, and cadmium. *RSC Adv.* **2016**, *6*, 24906–24911. [CrossRef]
25. Xia, Y.; Yang, T.; Zhu, N.; Li, D.; Chen, Z.; Lang, Q.; Liu, Z.; Jiao, W. Enhanced adsorption of Pb(II) onto modified hydrochar: Modeling and mechanism analysis. *Bioresour. Technol.* **2019**, *288*, 121593. [CrossRef]
26. Islam, M.A.; Ahmed, M.J.; Khanday, W.A.; Asif, M.; Hameed, B.H. Mesoporous activated coconut shell-derived hydrochar prepared via hydrothermal carbonization-NaOH activation for methylene blue adsorption. *J. Environ. Manag.* **2017**, *203*, 237–244. [CrossRef]
27. Islam, A.; Ahmed, M.; Khanday, W.A.; Asif, M.; Hameed, B. Mesoporous activated carbon prepared from NaOH activation of rattan (*Lacosperma secundiflorum*) hydrochar for methylene blue removal. *Ecotoxicol. Environ. Saf.* **2017**, *138*, 279–285. [CrossRef]
28. Petrović, J.; Stojanović, M.; Milojković, J.V.; Petrović, M.; Šoštarić, T.; Laušević, M.D.; Mihajlović, M.L. Alkali modified hydrochar of grape pomace as a perspective adsorbent of Pb 2+ from aqueous solution. *J. Environ. Manag.* **2016**, *182*, 292–300. [CrossRef]
29. Lv, B.W.; Xu, H.; Guo, J.Z.; Bai, L.Q.; Li, B. Efficient adsorption of methylene blue on carboxylate-rich hydrochar prepared by one-step hydrothermal carbonization of bamboo and acrylic acid with ammonium persulphate. *J. Hazard. Mater.* **2022**, *421*, 126741.
30. Zhou, N.; Chen, H.; Feng, Q.; Yao, D.; Chen, H.; Wang, H.; Zhou, Z.; Li, H.; Tian, Y.; Lu, X. Effect of phosphoric acid on the surface properties and Pb(II) adsorption mechanisms of hydrochars prepared from fresh banana peels. *J. Clean. Prod.* **2017**, *165*, 221–230. [CrossRef]
31. Marx, S.; Venter, R.J.; Louw, A.; Dewah, C.T. Upgrading of the aqueous product stream from hydrothermal liquefaction: Simultaneous removal of minerals and phenolic components using waste-derived hydrochar. *Biomass-Bioenergy* **2021**, *151*, 106170. [CrossRef]
32. Demir-Cakan, R.; Baccile, N.; Antonietti, M.; Titirici, M.M. Carboxylate-rich carbonaceous materials via one-step hy-drothermal carbonization of glucose in the presence of acrylic acid. *Chem. Mater.* **2009**, *21*, 484–490. [CrossRef]
33. Ghadikolaei, N.F.; Kowsari, E.; Balou, S.; Moradi, A.; Taromi, F.A. Preparation of porous biomass-derived hydrothermal carbon modified with terminal amino hyperbranched polymer for prominent Cr(VI) removal from water. *Bioresour. Technol.* **2019**, *288*, 121545. [CrossRef]
34. Takaya, C.; Fletcher, L.; Singh, S.; Anyikude, K.; Ross, A. Phosphate and ammonium sorption capacity of biochar and hydrochar from different wastes. *Chemosphere* **2016**, *145*, 518–527. [CrossRef]
35. Han, B.; Zhang, E.; Cheng, G.; Zhang, L.; Wang, D.; Wang, X. Hydrothermal carbon superstructures enriched with carboxyl groups for highly efficient uranium removal. *Chem. Eng. J.* **2018**, *338*, 734–744. [CrossRef]
36. Liu, J.-L.; Qian, W.-C.; Guo, J.-Z.; Shen, Y.; Li, B. Selective removal of anionic and cationic dyes by magnetic Fe3O4-loaded amine-modified hydrochar. *Bioresour. Technol.* **2021**, *320*, 124374. [CrossRef]
37. Liu, Z.; Wang, Z.; Chen, H.; Cai, T.; Liu, Z. Hydrochar and pyrochar for sorption of pollutants in wastewater and exhaust gas: A critical review. *Environ. Pollut.* **2021**, *268*, 115910. [CrossRef]

38. Li, B.; Guo, J.; Lv, K.; Fan, J. Adsorption of methylene blue and Cd(II) onto maleylated modified hydrochar from water. *Environ. Pollut.* **2019**, *254*, 113014. [CrossRef]
39. Li, B.; Lv, J.-Q.; Guo, J.-Z.; Fu, S.-Y.; Guo, M.; Yang, P. The polyaminocarboxylated modified hydrochar for efficient capturing methylene blue and Cu(II) from water. *Bioresour. Technol.* **2019**, *275*, 360–367. [CrossRef]
40. Li, H.Z.; Zhang, Y.N.; Guo, J.Z.; Lv, J.Q.; Huan, W.W.; Li, B. Preparation of hydrochar with high adsorption perfor-mance for methylene blue by cohydrothermal carbonization of polyvinyl chloride and bamboo. *Bioresour. Technol.* **2021**, *337*, 125442. [CrossRef]
41. Li, F.; Zimmerman, A.R.; Hu, X.; Yu, Z.; Huang, J.; Gao, B. One-pot synthesis and characterization of engineered hy-drochar by hydrothermal carbonization of biomass with ZnCl2. *Chemosphere* **2020**, *254*, 126866. [CrossRef]
42. Madduri, S.; Elsayed, I.; Hassan, E.B. Novel oxone treated hydrochar for the removal of Pb(II) and methylene blue (MB) dye from aqueous solutions. *Chemosphere* **2020**, *260*, 127683. [CrossRef]
43. Nguyen, D.H.; Tran, H.N.; Chao, H.-P.; Lin, C.-C. Effect of nitric acid oxidation on the surface of hydrochars to sorb methylene blue: An adsorption mechanism comparison. *Adsorpt. Sci. Technol.* **2019**, *37*, 607–622. [CrossRef]
44. Parra-Marfíl, A.; Ocampo-Pérez, R.; Collins-Martínez, V.H.; Flores-Vélez, L.M.; Gonzalez-Garcia, R.; Medellín-Castillo, N.A.; Labrada-Delgado, G.J. Synthesis and characterization of hydrochar from industrial Capsicum annuum seeds and its application for the adsorptive removal of methylene blue from water. *Environ. Res.* **2020**, *184*, 109334. [CrossRef]
45. Qian, W.-C.; Luo, X.-P.; Wang, X.; Guo, M.; Li, B. Removal of methylene blue from aqueous solution by modified bamboo hydrochar. *Ecotoxicol. Environ. Saf.* **2018**, *157*, 300–306. [CrossRef]
46. Ronix, A.; Pezoti, O.; de Souza, L.S.; Souza, I.P.A.F.; Bedin, K.C.; Souza, P.S.C.; Silva, T.L.; Melo, S.A.R.; Cazetta, A.L.; Almeida, V.C. Hydrothermal carbonization of coffee husk: Optimization of experimental parameters and adsorption of methylene blue dye. *J. Environ. Chem. Eng.* **2017**, *5*, 4841–4849. [CrossRef]
47. Tran, T.H.; Le, A.H.; Pham, T.H.; Nguyen, D.T.; Chang, S.W.; Chung, W.J.; Nguyen, D.D. Adsorption isotherms and kineticmodel-ing of methylene blue dye onto a carbonaceous hydrochar adsorbent derived from coffee husk waste. *Sci. Total Environ.* **2020**, *725*, 138325. [CrossRef]
48. Tran, H.N.; You, S.-J.; Chao, H.-P. Insight into adsorption mechanism of cationic dye onto agricultural residues-derived hydrochars: Negligible role of π-π interaction. *Korean J. Chem. Eng.* **2017**, *34*, 1708–1720. [CrossRef]
49. Li, B.; Wang, Q.; Guo, J.-Z.; Huan, W.-W.; Liu, L. Sorption of methyl orange from aqueous solution by protonated amine modified hydrochar. *Bioresour. Technol.* **2018**, *268*, 454–459. [CrossRef]
50. Spataru, A.; Jain, R.; Chung, J.W.; Gerner, G.; Krebs, R.; Lens, P.N.L. Enhanced adsorption of orthophosphate and copper onto hydrochar derived from sewage sludge by KOH activation. *RSC Adv.* **2016**, *6*, 101827–101834. [CrossRef]
51. Flora, J.F.; Lu, X.; Li, L.; Flora, J.R.; Berge, N.D. The effects of alkalinity and acidity of process water and hydrochar washing on the adsorption of atrazine on hydrothermally producedhydrochar. *Chemosphere* **2013**, *93*, 1989–1996. [CrossRef]
52. Machado, N.; de Castro, D.; Santos, M.; Araújo, M.; Lüder, U.; Herklotz, L.; Werner, M.; Mumme, J.; Hoffmann, T. Process analysis of hydrothermal carbonization of corn Stover with subcritical H_2O. *J. Supercrit. Fluids* **2018**, *136*, 110–122. [CrossRef]
53. Hoekman, S.K.; Broch, A.; Robbins, C.; Zielinska, B.; Felix, L. Hydrothermal carbonization (HTC) of selected woody and herbaceous biomass feedstocks. *Biomass-Convers. Biorefinery* **2012**, *3*, 113–126. [CrossRef]
54. Silva, C.D.M.S.D.; de Castro, D.A.R.; Santos, M.C.; Almeida, H.D.S.; Schultze, M.; Lüder, U.; Hoffmann, T.; Machado, N.T. Process analysis of main organic compounds dissolved in aqueous phase by hydrothermal processing of Açaí (Euterpe oleraceae, Mart.) Seeds: Influence of process temperature, biomass-to-water ratio, and production scales. *Energies* **2021**, *14*, 5608. [CrossRef]
55. Mota, S.; Mancio, A.D.A.; Lhamas, D.; de Abreu, D.; da Silva, M.; dos Santos, W.; de Castro, D.; de Oliveira, R.; Araújo, M.; Borges, L.E.; et al. Production of green diesel by thermal catalytic cracking of crude palm oil (Elaeis guineensis Jacq) in a pilot plant. *J. Anal. Appl. Pyrolysis* **2014**, *110*, 1–11. [CrossRef]
56. Almeida, H.D.S.; Corrêa, O.; Eid, J.; Ribeiro, H.; de Castro, D.; Pereira, M.; Pereira, L.; Mâncio, A.D.A.; Santos, M.; Souza, J.D.S.; et al. Production of biofuels by thermal catalytic cracking of scum from grease traps in pilot scale. *J. Anal. Appl. Pyrolysis* **2016**, *118*, 20–33. [CrossRef]
57. Serrão, A.C.M.; Silva, C.M.S.; Assunção, F.P.D.C.; Ribeiro, H.J.D.S.; Santos, M.C.; Almeida, H.D.S.; Junior, S.D.; Borges, L.E.P.; de Castro, D.A.R.; Machado, N.T. Análise do processo de pirólise de sementes de açaí (euterpe oleracea, mart): Influência da temperatura no rendimento dos produtos de reação e nas propriedades físico-químicas do bio-óleo/process analysis of pyrolise of açaí (euterpe oleracea, mart) seeds: Influence of temperature on the yield of reaction products and physico-chemical properties of bio-oil. *Braz. J. Dev.* **2021**, *7*, 18200–18220. [CrossRef]
58. Sittisun, P.; Tippayawong, N.; Wattanasiriwech, D. Thermal Degradation characteristics and kinetics of oxy combustion of corn residues. *Adv. Mater. Sci. Eng.* **2015**, *2015*, 1–8. [CrossRef]
59. Zhao, M.; Li, B.; Cai, J.-X.; Liu, C.; McAdam, K.; Zhang, K. Thermal & chemical analyses of hydrothermally derived carbon materials from corn starch. *Fuel Process. Technol.* **2016**, *153*, 43–49.
60. Kumar, S.; Kothari, U.; Kong, L.; Lee, Y.; Gupta, R.B. Hydrothermal pretreatment of switchgrass and corn stover for production of ethanol and carbon microspheres. *Biomass-Bioenergy* **2011**, *35*, 956–968. [CrossRef]
61. Yang, B.; Wyman, C.E. Effect of xylan and lignin removal by batch and flowthrough pretreatment on the enzymatic digestibility of corn stover cellulose. *Biotechnol. Bioeng.* **2004**, *86*, 88–98. [CrossRef]

62. Varga, E.; Szengyel, Z.; Réczey, K. Chemical pretreatments of corn stover for enhancing enzymatic digestibility. *Appl. Biochem. Biotechnol.* **2002**, *98*, 73–87. [CrossRef]
63. Mohammed, I.; Na, R.; Kushima, K.; Shimizu, N. Investigating the effect of processing parameters on the products of hydrothermal carbonization of corn stover. *Sustainability* **2020**, *12*, 5100. [CrossRef]
64. Xing, X.; Fan, F.; Shi, S.; Li, Y.; Zhang, X.; Yang, J. Fuel properties and combustion kinetics of hydrochar prepared by hydrothermal carbonization of corn straw. *BioResources* **2016**, *11*, 9190–9204. [CrossRef]
65. Hoskinson, R.L.; Karlen, D.L.; Birrell, S.J.; Radtke, C.W.; Wilhelm, W.W. Engineering, nutrient removal, and feedstock conversion evaluations of four corn stover harvest scenarios. *Biomass Bioenergy* **2007**, *31*, 126–136. [CrossRef]
66. Kang, K.; Sonil, N.; Guotao, S.; Ling, Q.; Yongqing, G.; Tianle, Z.; Mingqiang, Z.; Runcang, S. Microwaveassisted hydrothermal carbonizatijon of corn stalk for solid biofuel production: Optimization of process parameters and characterization of hydrochar. *Energy* **2019**, *186*, 115–125. [CrossRef]
67. Becker, R.; Dorgerloh, U.; Helmis, M.; Mumme, J.; Diakité, M.; Nehls, I. Hydrothermally carbonized plant materials: Patterns of volatile organic compounds detected by gas chromatography. *Bioresour. Technol.* **2013**, *130*, 621–628. [CrossRef] [PubMed]
68. Reza, M.T.; Wirth, B.; Lueder, U.; Werner, M. Behavior of selected hydrolyzed and dehydrated products during hydrothermal carbonization of biomass. *Bioresour. Technol.* **2014**, *169*, 352–361. [CrossRef] [PubMed]
69. Liang, J.; Liu, Y.; Zhang, J. Effect of solution pH on the carbon microsphere synthesized by hydrothermal carbonization. *Procedia Environ. Sci.* **2011**, *11*, 1322–1327. [CrossRef]